Distinct brain networks for adaptive and stable task control in humans

Nico U. F. Dosenbach*†, Damien A. Fair‡, Francis M. Miezin*‡, Alexander L. Cohen*, Kristin K. Wenger‡, Ronny A. T. Dosenbach*‡, Michael D. Fox*, Abraham Z. Snyder*‡, Justin L. Vincent*, Marcus E. Raichle*†‡§, Bradley L. Schlaggar*‡§¶, and Steven E. Petersen*†‡§‖

Departments of *Radiology, ‡Neurology, §Neurobiology and Anatomy, ¶Pediatrics, and ‖Psychology, Washington University, St. Louis, MO 63110

Contributed by Marcus E. Raichle, May 8, 2007 (sent for review March 28, 2007)

Control regions in the brain are thought to provide signals that configure the brain's moment-to-moment information processing. Previously, we identified regions that carried signals related to task-control initiation, maintenance, and adjustment. Here we characterize the interactions of these regions by applying graph theory to resting state functional connectivity MRI data. In contrast to previous, more unitary models of control, this approach suggests the presence of two distinct task-control networks. A frontoparietal network included the dorsolateral prefrontal cortex and intraparietal sulcus. This network emphasized start-cue and error-related activity and may initiate and adapt control on a trial-by-trial basis. The second network included dorsal anterior cingulate/medial superior frontal cortex, anterior insula/frontal operculum, and anterior prefrontal cortex. Among other signals, these regions showed activity sustained across the entire task epoch, suggesting that this network may control goal-directed behavior through the stable maintenance of task sets. These two independent networks appear to operate on different time scales and affect downstream processing via dissociable mechanisms.

attention | connectivity | executive control | functional MRI | task set

Humans possess unrivaled cognitive flexibility. When performing goal-directed tasks, humans are thought to adopt task sets that flexibly configure information processing in response to changing task demands. The brain's task-control system is thought to consist of functionally diverse regions that are anatomically separate from downstream processing systems (1).

Previously, we studied mixed blocked/event-related fMRI data across a wide range of tasks (2). Because mixed fMRI designs can disambiguate sustained set-maintenance activity from more transient set and trial-related activity (3, 4), we were able to identify regions that carried three different putative task-control signals: (*i*) activity time-locked to the beginning of task periods (control initiation), (*ii*) set-maintenance signals sustained across the entire task period, and (*iii*) error-related activity (for feedback and control adjustment). Using cross-studies analyses, we identified a collection of regions thought to support these various task-control signals.

The dorsal anterior cingulate cortex/medial superior frontal cortex (dACC/msFC) and bilateral anterior insula/frontal operculum (aI/fO) were the only regions that showed all three task-control signals (set initiation, maintenance, and feedback and adjustment) across a wide range of tasks. Therefore, we proposed that the dACC/msFC and aI/fO might form the "core" of a system for task set implementation (2, 5). Other regions of interest (ROIs), such as the anterior prefrontal cortex (aPFC), dorsolateral prefrontal cortex (dlPFC), and inferior parietal lobule (IPL), previously implicated in various control functions (6–10), carried different combinations of signals in different sets of tasks, including considerably less evidence of sustained activity. Based on these fMRI activation results (2), a single centralized control system anchored by the "core" regions (dACC/msFC, aI/fO), which also included aPFC and dlPFC, was proposed (Fig. 1*A*).

The ability to perform myriad tasks requires control functions that persist across time and prevail against distraction, but can also respond quickly to unpredictable demands that arise during task performance. In contrast to previous models of control (2, 11, 12), including that proposed in Fig. 1*A*, complex adaptive systems models favor multiple "controlling variables" often occurring on different time scales over more centralized control because they offer greater resilience and flexibility. Thus, "faster levels invent, experiment, and test; the slower levels stabilize and conserve accumulated memory of past successful, surviving experiments" (13).

Our activation data alone were insufficient for making strong inferences about the presence or absence of multiple control systems. To test our "core" model (Fig. 1*A*) against a multiple control architecture predicted by complex systems theory, we felt the need to learn more about the interregional interactions between the putative task-control regions we had identified previously. In the current study, we elucidated the functional integration of task-control regions in terms of the correlation structure of their blood oxygenation level-dependent signal (BOLD) activity. The field has settled on at least two types of approaches to the analysis of interregional correlations in BOLD activity. One approach is to examine the effective connectivity temporarily induced by manipulating the demands of a specific task (12). A second option is to employ resting state functional connectivity MRI (rs-fcMRI) (14–22), which is the method used in this paper.

rs-fcMRI measurements are based on the observation that spontaneous low-frequency (<0.1 Hz) BOLD fluctuations in distant, but functionally related, gray matter regions are correlated at rest (16, 21–23) (Fig. 1*B*). Resting functional connectivity was first described in the motor system (14). Important validation studies have since confirmed that resting state fluctuations are large in magnitude (% of BOLD signal change) and highly consistent across subjects (21, 22).

Seed-based connectivity methods, for example, allow one to map the resting state correlations of a single-seed region with every other voxel in the brain (Fig. 1*C*). Such seed-based maps reliably reveal biologically plausible relationships between brain regions in humans (20) and macaques (24). For example, placing a seed in the right aI/fO reveals its functional connections to the left aI/fO and the dACC/msFC (Fig. 1*C*).

Given these observations, one reasonable speculation regarding correlations in spontaneous BOLD fluctuations between brain

Author contributions: N.U.F.D. and S.E.P. designed research; N.U.F.D. performed research; M.D.F., A.Z.S., J.L.V., and M.E.R. contributed new reagents/analytic tools; N.U.F.D., D.A.F., F.M.M., A.L.C., K.K.W., R.A.T.D., and B.L.S. analyzed data; and N.U.F.D., D.A.F., B.L.S., and S.E.P. wrote the paper .

The authors declare no conflict of interest.

Abbreviations: aI/fO, anterior insula/frontal operculum; aPFC, anterior prefrontal cortex; BOLD, blood oxygenation level-dependent signal; Cp, clustering coefficient; dACC/msFC, dorsal anterior cingulate cortex/medial superior frontal cortex; dlPFC, dorsolateral prefrontal cortex; IPL, inferior parietal lobule; IPS, intraparietal sulcus; Lp, path length; ROI, region of interest; rs-fcMRI, resting state functional connectivity MRI.

†To whom correspondence may be addressed. E-mail: ndosenbach@wustl.edu, marc@npg.wustl.edu, or sep@npg.wustl.edu.

This article contains supporting information online at www.pnas.org/cgi/content/full/0704320104/DC1.

NEUROSCIENCE

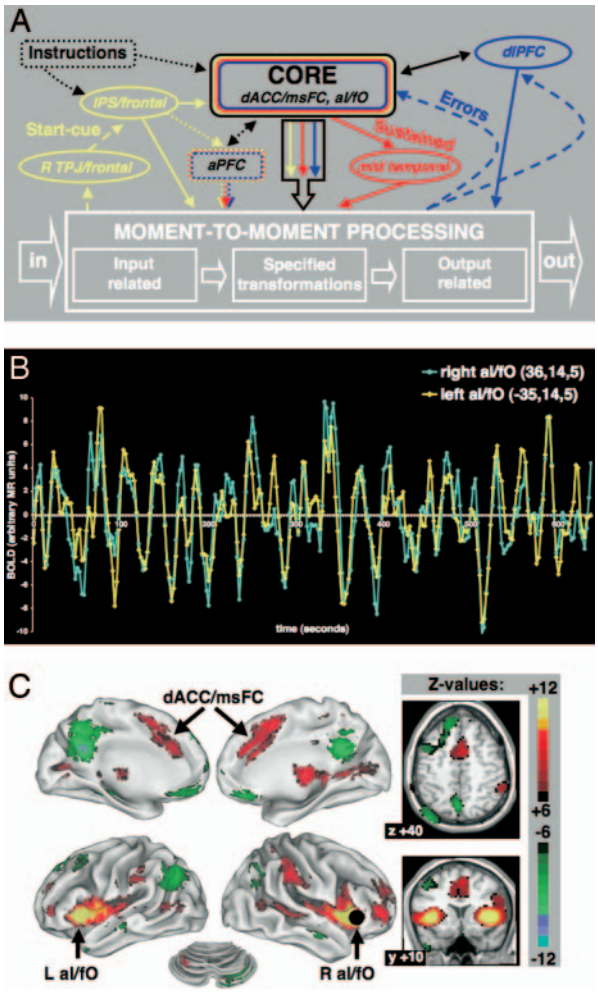

Fig. 1. Analyzing interactions between predefined task-control regions using rs-fcMRI. (*A*) Old hypothetical framework of centralized control system based on multistudy (10 tasks, 183 subjects) analyses. [Reproduced with permission from ref. 2 (Copyright 2006, Elsevier).] Control initiation (yellow), set maintenance (red), and feedback/control adjustment (blue). (*B*) rs-fcMRI is measured by calculating the correlations in spontaneous BOLD fluctuations between brain regions. Spontaneous resting state BOLD fluctuations for two sample regions (right aI/fO and left aI/fO), measured in a single subject. (*C*) Voxelwise rs-fcMRI map for a sample seed region, R aI/fO (4, 16, 36).

regions is that they may, at least in part, reflect a longstanding history of coactivation. Consistent with Hebbian mechanisms (25), repeated coactivation during everyday activity may have led to greater synaptic efficiencies between certain regions, causing their spontaneous BOLD fluctuations to be consistently correlated. The relative contributions of "synaptic modifications" and the underlying "connectional anatomy" to rs-fcMRI patterns remain to be determined.

To characterize the interregional relations for our predefined ROIs (2), we applied graph theory (18, 19, 26) to a large resting BOLD data set (74 young adults). Graph theory defines a graph as a set of nodes (in this study, ROIs) and edges (functional connections). By focusing on region pairs, this approach allowed us to simultaneously visualize the connectivity structure of a large number of ROIs. Graphs can also identify groups or "components" of regions that are disconnected from all other nodes in the graph, as well as highly connected network "hubs" (27). Graph theory has been used to characterize complex systems as diverse as the U.S. power grid, *Caenorhabditis elegans'* neuronal networks (28), and anatomical connections of the macaque visual system (29).

Table 1. ROIs sorted into components based on rs-fcMRI

	Coordinates				Sustained			
ROI	*x*	*y*	*z*	Comp	Neg	Pos	Cue	Err
R IPS	30	−61	39	1			X	
L IPS	−31	−59	42	1			X	
R frontal cortex	41	3	36	1			X	
L frontal cortex	−41	3	36	1				
R precuneus	10	−69	39	1			X	
L precuneus	−9	−72	37	1			X	
midcingulate	0	−29	30	1			X	
R IPL	51	−47	42	1				X
L IPL	−51	−51	36	1		X		
R dlPFC	43	22	34	1				X
L dlPFC	−43	22	34	1				
R aI/fO	36	16	4	2		X	X	X
L aI/fO	−35	14	5	2		X	X	X
dACC/msFC	−1	10	46	2		X	X	X
R aPFC*	27	50	23	2		X*	X*	X
L aPFC*	−28	51	15	2		X*	X*	X
R ant thalamus	10	−15	8	2			X	X
L ant thalamus	−12	−15	7	2				X
R lat cerebellum	31	−61	−29	3				X
L lat cerebellum	−32	−66	−29	3				X
R inf cerebellum	18	−80	−33	3				X
L inf cerebellum	−19	−78	−33	3				X
R TPJ	53	−46	17	4			X	
L TPJ	−53	−46	17	4				
R midoccipital	27	−89	3	5				
L midoccipital	−27	−89	3	5	X		X	
R lingual	8	−82	4	5			X	
L lingual	−8	−82	4	5			X	
R posttemporal	44	−74	26	6	X			
L posttemporal	−40	−78	24	6	X			
R postcingulate	10	−56	16	6	X			
L postcingulate	−11	−57	13	6	X			
R fusiform	35	−65	−9	6			X	
L fusiform	−34	−62	−15	6			X	
R ant fusiform	25	−44	−12	6				
L ant fusiform	−25	−44	−12	6	X			
R midtemporal	51	−33	−2	7		X		
L midtemporal	−53	−31	−5	7		X		
vmPFC	1	31	−2	8	X			

*Only for subset of 10 tasks included in cross-studies analyses.

Results

Thirty-nine putative task-control ROIs (Table 1) were derived from the previous cross-studies analyses described above (2). Pairwise BOLD correlations (functional connections) were extracted for this set of ROIs to generate a correlation matrix (see *Materials and Methods*).

Graph Analysis. We created unweighted, binary graphs such that nodes were either connected or not connected. Future analyses might take connection weights into account (29). The distribution of r values suggested a natural division at $r = 0.2$ and led us to first threshold the correlation matrix at $r \geq 0.2$ [supporting information (SI) Fig. 5]. All interregional correlations with $r \geq 0.2$ were statistically significant at $P < 10^{-9}$ (two-tailed; Bonferroni corrected; t test).

Graph Metrics. The graph defined by the $r \geq 0.2$ threshold was sparse (Fig. 2*A* and SI Fig. 6*A*). It contained only ≈8% of all possible connections (61 edges). The structure of this task-control graph differed strongly from both completely random and completely regular graphs with the same number of regions and connections (SI Fig. 6) classically used for structural comparisons (28). The task-control graph separated into eight disconnected components, whereas 100 randomly generated graphs contained on average

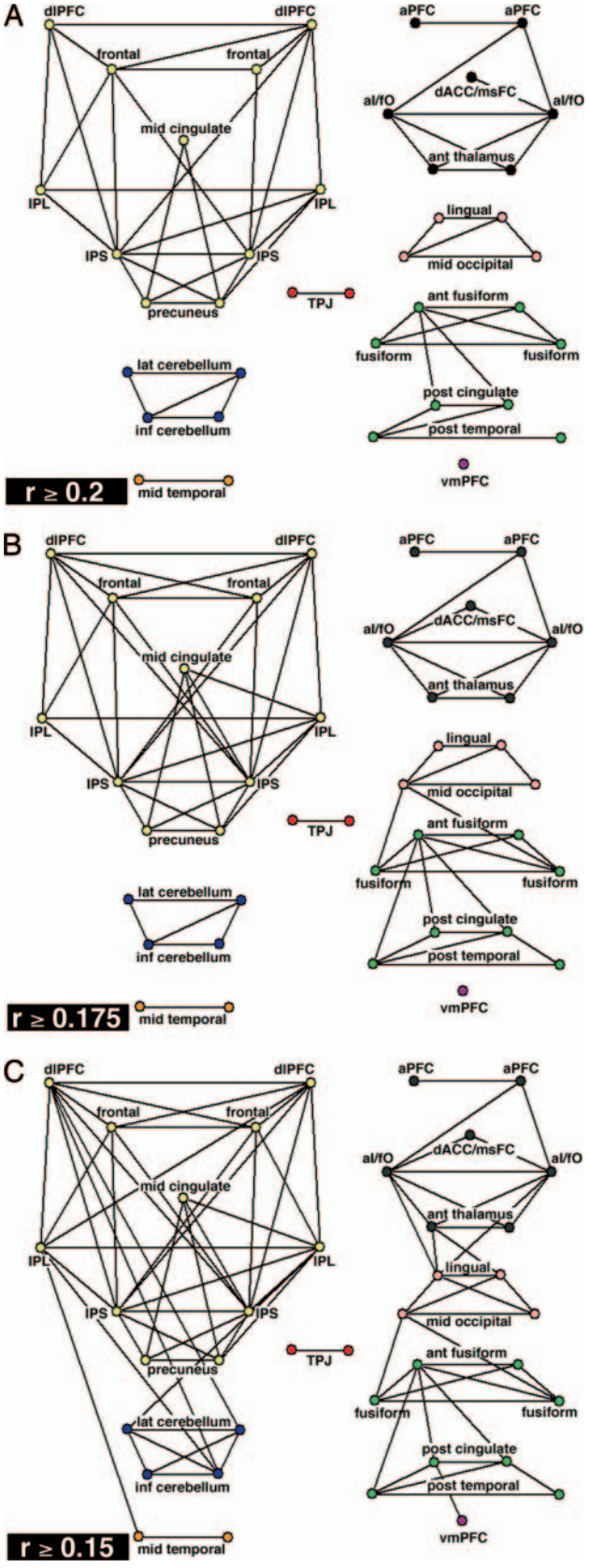

Fig. 2. Task-control graphs across different thresholds. 2D pseudoanatomical renderings of task-control graphs. (*A*) Thresholded at $r \geq 0.2$ ($P < 1 \times 10^{-9}$; two-tailed; Bonferroni corrected; *t* test). (*B*) Thresholded at $r \geq 0.175$ ($P < 1 \times 10^{-7}$; two-tailed; Bonferroni corrected; *t* test). (*C*) Thresholded at $r \geq 0.15$ ($P < 5 \times 10^{-5}$; two-tailed; Bonferroni corrected; *t* test).

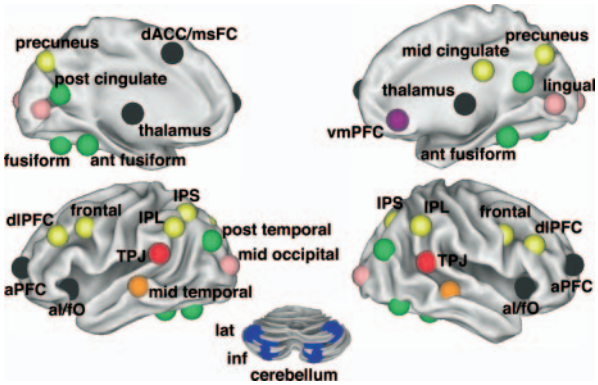

Fig. 3. Task-control graph components ($r \geq 0.2$) on the brain. Eight separate components that constitute task-control graph ($r \geq 0.2$) displayed on inflated surface rendering of the brain. Nodes are color-coded by components in Fig. 2*A*. Interregional correlations were significant at $P < 1 \times 10^{-9}$ (two-tailed; Bonferroni corrected; *t* test).

1.9 ± 0.5 (SD) components (SI Fig. 6*B*). Completely regular "lattice" graphs always consist of a single component (SI Fig. 6*C*).

The eight components were strongly connected within themselves as reflected by the very high clustering coefficient [(Cp) 0.57; see *Materials and Methods*], a metric for the local "intraconnectedness" of neighborhoods within a graph (28). The Cp for the task-control graph was similar to that of a comparable regular graph (0.63) and much greater than the average Cp of random graphs (0.07 ± 0.04 SD).

The characteristic path length [(Lp), the shortest path connecting regions averaged across all pairs of regions] of the task-control graph was much smaller (Lp = 1.43) than that of comparable random (Lp = 3.0 ± 0.15 SD) and regular (Lp = 5.4) graphs (SI Table 2 and SI Fig. 7). The large Cp and short characteristic Lp further indicated that the task-control graph consisted of several distinct and "clumpy" components (28).

Graph Components. The largest component (Figs. 2*A* and 3) consisted of 11 ROIs in frontal and parietal cortex (frontoparietal component). The intraparietal sulcus (IPS) belonged to this component, as did the frontal cortex, dlPFC, IPL, precuneus, and midcingulate cortex.

The three regions hypothesized to form the "core" of a human task-set system (dACC/msFC, left aI/fO, and right aI/fO) (2) were part of a second component (Figs. 2*A* and 3). Bilateral aPFC, previously implicated in set maintenance (6, 7, 10, 30, 31), also belonged to this component, as did bilateral regions in the anterior part of the thalamus. For simplicity, we refer to this second component (dACC/msFC, aI/fO, aPFC, and thalamus) as the cinguloopercular component.

The remaining components were not as clearly related to task control (Fig. 3). Four cerebellar regions that had all shown error-related activity in the cross-studies analyses of fMRI activations (2) formed a separate component. Another component consisted of four occipital regions. An eight-ROI component consisted of fusiform regions and parts of the brain's default network (32).

To determine how these findings were affected by changes in the graph-definition threshold, lower *r*-value thresholds were also analyzed (Fig. 2). Lowering the graph analysis threshold to $r \geq 0.175$ increased the number of edges to 71 (Fig. 2*B*). The number of components decreased from eight to seven (random: 1.6 ± 0.54 SD) because the occipital component became connected to the default/fusiform component. Overall, the graphs generated by thresholding at $r \geq 0.2$ and $r \geq 0.175$ were similar, indicating that our findings are robust to small changes in the graph-definition threshold.

Further decreasing the threshold to $r \geq 0.15$ increased the

NEUROSCIENCE

number of connections to 85 and lowered the number of components to three (Fig. 2*C*). One component combined the frontoparietal, cerebellar, and middle temporal regions. A second component consisted of the cinguloopercular, occipital, and fusiform regions. Even at the $r \geq 0.15$ threshold, the cinguloopercular and frontoparietal ROIs remained in separate components.

More important, the frontoparietal and cinguloopercular components also differed in their connection patterns to other parts of the brain. At $r \geq 0.15$, the IPL and dlPFC became connected to cerebellar regions. In contrast, cinguloopercular regions (aI/fO, thalamus) became connected to putative downstream sensory regions in the occipital cortex (L, −8, −82, 4; R, 8, −82, 4).

Lowering the graph definition threshold did not randomly add additional connections. Instead, the highly intraconnected clumps (large Cp) became still more strongly intraconnected, and some interclump short cuts appeared between "bridge" regions (Fig. 2*C* and SI Fig. 8). Furthermore, the task-control graphs always retained structure different from both completely random and completely regular even when the graph-definition thresholds were lowered further to $r \geq 0.125$ and $r \geq 0.1$ (SI Table 2 and SI Fig. 8).

Validation of Graph Results Using Hierarchical Clustering. Hierarchical clustering (SI Fig. 9) generated eight clusters that were strikingly similar to the eight components generated by the ($r \geq 0.2$) graph analysis (SI Fig. 10). The cinguloopercular, frontoparietal, cerebellar, occipital, and temporoparietal junction components from the graph analysis mapped precisely onto the clustering results (see *SI Text*). The strong convergence between the graph and clustering results demonstrates that our findings are independent of the specific analysis method.

Discussion

The principal finding of the present study is that humans possess separable frontoparietal and cinguloopercular networks with disparate resting state connectivity patterns. These networks also show disparate functional properties (2). Our study showed that the network structure is "clumpy," with Cps as high as those of completely regular graphs, but with shorter Lps. At all graph definition thresholds tested, the pattern of functional connections was far from random (27). Even at lower correlation thresholds ($r \geq 0.15$), no path connected the frontoparietal and cinguloopercular ROIs. Further, there was strong "intraconnectedness" within the sets of ROIs and a lack of connections between the sets.

Based on the differences in their connectivity and activation profiles, we propose that these networks support distinct adaptive control (frontoparietal) and stable set-maintenance (cinguloopercular) functions. We suggest that this "dual-network" account of task control better captures the phenomenology than previous "unitary" models of executive control (e.g., see refs. 2 and 11).

To discuss the possible functions of the frontoparietal and cinguloopercular networks in detail, we combine connectivity information with activation profiles from prior activation studies (2) summarized in Table 1.

Frontoparietal Network: Active, Adaptive Online Control. The IPS, precuneus, midcingulate, and lateral frontal cortex carried only start cue-related activity. The right IPL and dlPFC carried only error-related activity. Further, only 1 of the 11 ROIs in the frontoparietal network showed sustained activity across tasks (left IPL; see Table 1). This activation profile suggests that the frontoparietal network may support control initiation and provide flexibility by adjusting control in response to feedback. The frontoparietal adaptive control network appears to include the dorsal attention network proposed by Corbetta *et al.* (33). The dorsal attention network seems to be functionally connected to the IPL and dlPFC, regions previously implicated in control (9, 34, 35).

The IPS is thought to play a major role in the top–down control of attention (33). Our finding that the IPS occupies a central integrative position in the frontoparietal network (SI Fig. 11) is consistent with the notion that the frontoparietal network exerts top–down control. Imaging studies of attention have shown the precuneus and midcingulate cortex to be coactivated with the IPS and lateral frontal cortex (36). A study by Woldorff *et al.* (36) showed that the IPS (coordinates: L, −28, −62, 41; R, 32, −61, 45) and lateral frontal cortex (coordinates: L, −48, 3, 43; R, 46, 6, 43) were active when a cue was interpreted but attention was not shifted, whereas the precuneus was only active when attention was shifted.

The frontal region (41, 3, 36) we identified appears to be situated somewhat inferior to the human homologue of the frontal eye fields. Closely adjacent regions in the frontal cortex have been suggested to help direct motor attention (37). Therefore, the IPS and frontal cortex may decode the meaning of cues, and the precuneus and midcingulate may help direct selective attention.

It is thought that the dlPFC aids in the adjustment of top–down control in response to feedback (e.g., errors) by integrating information from one trial to the next, often over many seconds (11). Consistent with activation studies that showed the dlPFC's activation profile to be similar to the IPL's (2, 34), the current study demonstrates that the dlPFC is functionally connected to the IPL. A recent fMRI study by Liston *et al.* (9) demonstrated that a region in the right posterior parietal cortex (coordinates: 53, −38, 40), close to our IPL region (coordinates: 51, −47, 42), was sensitive to conflict at the level of stimulus presentation (9). Liston *et al.* suggested that the posterior parietal cortex might signal stimulus conflict to the dlPFC, which then adjusts control parameters accordingly.

Both the dlPFC and IPL were functionally connected to error-responsive cerebellar regions (Fig. 2*C*). Consistent with the crossed nature of connectional anatomy between the cerebellum and cortex, right cerebellar regions were functionally connected to the left frontal and parietal regions and vice versa. Previous work indicates that the cerebellum may generate error codes (see ref. 38), suggesting that the IPL and dlPFC might receive cerebellar error signals that support the rapid, continual fine-tuning of control settings and decision making (Fig. 4).

Cinguloopercular Network: Stable Maintenance of Task Mode and Strategy. The cinguloopercular network included all of the ROIs that had previously shown overlap of task initiation, maintenance, and monitoring/adjustment signals, along with the thalamus (Table 1). The major functional distinctions between the cinguloopercular and frontoparietal control networks were this overlap across control signals and the much greater prevalence of longer acting, across-trial set-maintenance activity in the cinguloopercular network. Therefore, we propose that the cinguloopercular network contributes to the flexible control of human goal-directed behavior through the stable, across-trial implementation of task sets in downstream sensorimotor processors (Fig. 4). Consistent with this hypothesis, the cinguloopercular network was functionally connected to putative downstream processors in occipital cortex (Fig. 2*C*). These occipital regions in turn were functionally connected to other posterior regions in fusiform and extrastriate cortex (Fig. 2*C*).

As discussed below, the combination of results presented here and in the literature suggests that the dACC/msFC and aI/fO "core" might in part support a basic domain-independent and externally directed "task mode" (5) in opposition to the brain's "default mode" (32), whereas the aPFC might provide more specific representations of plans, subgoals (39), rules (10, 40), and/or strategies (31) for complex task paradigms. The cinguloopercular network we identified thus unifies a set of regions (aPFC, dACC/msFC, aI/fO) individually associated with different executive functions, such as rule maintenance (40) and performance monitoring (41). Although previously debated (1, 11), recent studies in humans (2, 35, 42–44) and macaques (45, 46) have demonstrated preparatory and maintenance control signals in the dACC/msFC, indicating that the

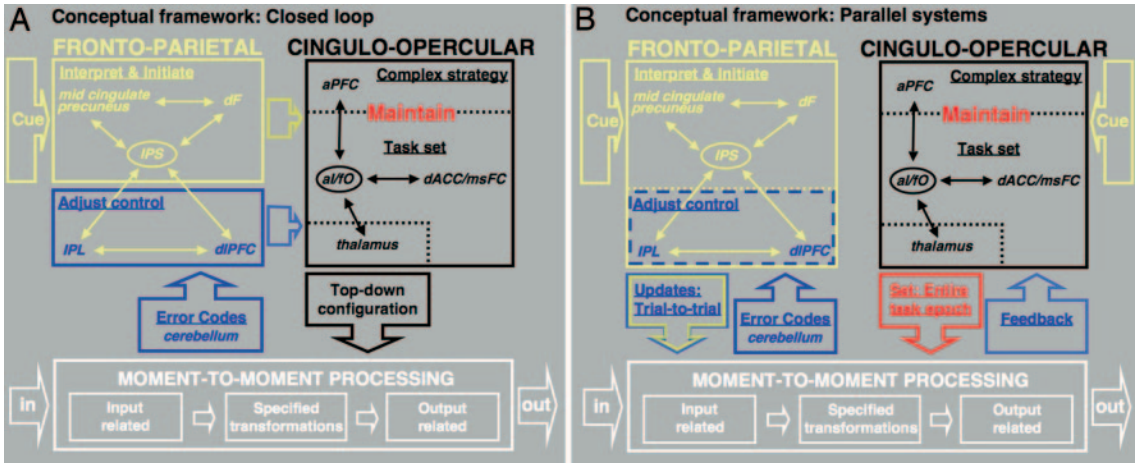

Fig. 4. Dual-network hypothesis of task control. Thin arrows schematize strong functional connections, ovals schematize hubs, and thick arrows schematize putative flow of information. (*A*) Information may flow between the frontoparietal and cinguloopercular networks, such that the stable control network receives control initiation signals from the adaptive control network at the beginning of a task period, as well as adjustment signals during task performance. (*B*) Alternatively, the frontoparietal and cinguloopercular control networks may be organized in parallel. Both networks might interpret cues, implement top–down control, and process bottom–up feedback. The frontoparietal network may adjust task control on a trial-by-trial basis, whereas the cinguloopercular network might affect downstream processing in a more stable fashion. Frameworks intermediate between *A* and *B* are also consistent with the data.

dACC/msFC actively exerts top–down control over sensory (47) and limbic brain regions (48).

In contrast, the aI/fO has received less attention as a potential task-control region (2, 49). The aI/fO, sometimes labeled ventrolateral prefrontal cortex or anterior ventrolateral prefrontal cortex, has been present in several imaging experiments that measured control signals (10, 40, 50). Important studies in humans and nonhuman primates have implicated the aI/fO in the representation of task rules (8, 49). Consistent with a central role in task control, the aI/fO connectivity profile identified it as a hub of the proposed human cinguloopercular network (SI Fig. 11).

Prior studies have associated the aPFC (lateral area 10) with complex higher order task-control functions (39, 51). Sakai *et al.* (30) reported extended task set-related activity in aPFC (L, −30, 56, 4; R, −32, 56, 8) that appeared to be domain-dependent (30). Other fMRI experiments have shown that the aPFC is more active when subjects have to switch between task sets (6) or implement complex rules (40). It seems reasonable that regions (dACC/msFC, aI/fO) central to the implementation of a domain-general task mode would be strongly functionally connected to regions important for the implementation of complex task rules and strategies, such as the aPFC.

Possible Interactions Between the Frontoparietal and Cinguloopercular Networks. The frontoparietal and cinguloopercular control networks were strongly intraconnected and quite separate from each other (Fig. 2*C* and SI Figs. 8–10), suggesting that they carry out dissociable control functions. The networks may nonetheless communicate with each other (Fig. 4*A*). The frontoparietal network may provide the cinguloopercular network with more rapid control initiation and adjustment signals, whereas the cinguloopercular network may maintain set throughout the entire task period to affect downstream processing.

If the frontoparietal and cinguloopercular networks were to communicate, why did none of our large-scale analyses reveal a link between them? Our analyses were limited to a set of 39 predefined ROIs. Therefore, we may not have included an additional member of both networks that could act as a specialized information transfer "bridge" between them. By adding additional functionally defined ROIs to our analysis stream, we might be able to identify paths that functionally connect the frontoparietal and cinguloopercular networks. We expect a significantly larger set of ROIs (>39) to form a single "small-world" network (19, 29) that consists of several dense clumps held together via long-range short cuts, maintaining relative separateness among the components.

Some studies have suggested transient correlations in BOLD signal between the dACC and dlPFC during difficult dual-task situations (52). Although dual-task situations may temporarily induce interactions between the dACC and dlPFC, such situations may not occur frequently enough to have generated long-term resting connectivity between the two control networks.

Across a series of activation studies (2), functional dissociations were apparent between members of the two networks. Therefore, the two control networks may well function in parallel (Fig. 4*B*). Both networks might exert parallel top–down control over downstream processing, albeit through different mechanisms. In such a framework, both the adaptive (frontoparietal) and stable (cinguloopercular) task-control networks would independently interpret cues and receive bottom–up performance feedback signals. The frontoparietal network would maintain control signals online in working memory from one or a small number of trials to the next, enabling it to implement task control on a faster trial-to-trial basis. The cinguloopercular network, in contrast, would implement and update basic task sets only on a slower time scale.

One potential advantage of a more parallel organization would be increased resiliency to perturbation or damage. Many complex systems in nature seem to be affected by different "control variables" that can operate at different time scales and exert control through relatively separate mechanisms (13). Further research is needed to decide between the interactive (Fig. 4*A*) and parallel (Fig. 4*B*) alternatives for top–down control or possible hybrid organizations. Our current data seem most consistent with a more parallel architecture.

Materials and Methods

Data Acquisition and Processing. All functional imaging data were obtained on the same 1.5 Tesla scanner and processed exactly as described previously in Miezin *et al.* (53). Details can be found in *SI Text*.

Functional Connectivity Preprocessing. Preprocessing for functional connectivity analyses was carried out exactly as previously described (20) (see *SI Text*).

ROI Definition. Thirty-nine ROIs were derived from cross-studies analyses (183 subjects, 10 tasks) of task-control signals by creating 12-mm diameter spheres around previously identified center of mass coordinates (2). See *SI Text* for further details.

Extraction of Regionwise Resting State Time Series. Resting state (fixation) data from 74 young adults (18–35 years old) were included in the analyses. For each subject, at least 256 TRs (640 sec) of fixation resting state BOLD data were available. For each of the 39 ROIs, a resting state time series was extracted separately for each individual. For 10 of the subjects, the resting data (fixation) were continuous. For the remaining 64 subjects, the resting periods (fixation) were taken from different interleaved experimental designs that also contained task periods. Our method for extracting resting periods from blocked fMRI designs was validated in a recent study (54).

Generation of Seed-Based Resting Functional Connectivity Maps. Voxelwise resting state functional connectivity statistical maps (Fig. 1*C*) were generated by using a random effects approach as previously described (15).

Computation of Mean Regionwise Correlation Matrix. The resting state BOLD time series were correlated region by region for each subject across the full length of the resting time series, creating 74 square correlation matrices (39×39). To combine correlation coefficients (r) across subjects, the Schmidt–Hunter method for metaanalyses of r values was used because it is more conservative than comparable methods (18, 55).

We performed 741 one-sample t tests (two-tailed) on Fisher's Z-transformed (normally distributed) correlation coefficients to test whether they were significantly different from zero (18). To account for multiple comparisons, Bonferroni's correction was applied.

Graph Analysis. All graph theoretical calculations were performed in Matlab 7.2 (Natick, MA). The algorithms for computing graph theoretical metrics were based on those generously made available by Olaf Sporns (www.indiana.edu/%7Ecortex/connectivity_toolbox.html) (27). We only used unweighted undirected graphs, and we did not allow for regions to be connected to themselves.

All graph theoretical metrics were calculated for the original graph as well as 100 completely random graphs (SD) and a regular lattice graph, as first introduced by Watts *et al.* (28). In a regular or lattice graph, each region is only connected to the next regions around the ring. Because graph measures can be sensitive to node degree, we generated a second set of randomized and latticized controls for which the node degrees were preserved (29) (SI Table 3). The graph analysis conclusions were unaffected by node degree preservation. Graphs were visualized using Pajek (www.vlado.fmf.uni-lj.si/pub/networks/pajek).

We thank Steven M. M. Nelson and Jessica A. Church for helpful discussion and Mark McAvoy for help with data analysis. This work was supported by National Institutes of Health Grants NS41255 and NS46424 (to S.E.P.), the John Merck Scholars Fund, the Burroughs-Wellcome Fund and the Dana Foundation (B.L.S.), and the Washington University Chancellor's Fellowship and UNCF Merck Graduate Science Research Dissertation Fellowship (to D.A.F.).

1. Posner MI, Petersen SE (1990) *Annu Rev Neurosci* 13:25–42.
2. Dosenbach NU, Visscher KM, Palmer ED, Miezin FM, Wenger KK, Kang HC, Burgund ED, Grimes AL, Schlaggar BL, Petersen SE (2006) *Neuron* 50:799–812.
3. Chawla D, Rees G, Friston KJ (1999) *Nat Neurosci* 2:671–676.
4. Visscher KM, Miezin FM, Kelly JE, Buckner RL, Donaldson DI, McAvoy MP, Bhalodia VM, Petersen SE (2003) *Neuroimage* 19:1694–1708.
5. Braver TS, Barch DM (2006) *Trends Cogn Sci* 10:529–532.
6. Braver TS, Reynolds JR, Donaldson DI (2003) *Neuron* 39:713–726.
7. Sakai K, Passingham RE (2003) *Nat Neurosci* 6:75–81.
8. Badre D, Wagner AD (2004) *Neuron* 41:473–487.
9. Liston C, Matalon S, Hare TA, Davidson MC, Casey BJ (2006) *Neuron* 50:643–653.
10. Crone EA, Wendelken C, Donohue SE, Bunge SA (2006) *Cereb Cortex* 16:475–486.
11. Miller EK, Cohen JD (2001) *Annu Rev Neurosci* 24:167–202.
12. Koechlin E, Ody C, Kouneiher F (2003) *Science* 302:1181–1185.
13. Gunderson LH, Holling CS (2002) *Panarchy: Understanding Transformations in Human and Natural Systems* (Island Press, Washington, DC).
14. Biswal B, Yetkin FZ, Haughton VM, Hyde JS (1995) *Magn Reson Med* 34:537–541.
15. Vincent JL, Snyder AZ, Fox MD, Shannon BJ, Andrews JR, Raichle ME, Buckner RL (2006) *J Neurophysiol* 96:3517–3531.
16. Lowe MJ, Mock BJ, Sorenson JA (1998) *Neuroimage* 7:119–132.
17. Greicius MD, Krasnow B, Reiss AL, Menon V (2003) *Proc Natl Acad Sci USA* 100:253–258.
18. Salvador R, Suckling J, Coleman MR, Pickard JD, Menon D, Bullmore E (2005) *Cereb Cortex* 15:1332–1342.
19. Achard S, Salvador R, Whitcher B, Suckling J, Bullmore E (2006) *J Neurosci* 26:63–72.
20. Fox MD, Corbetta M, Snyder AZ, Vincent JL, Raichle ME (2006) *Proc Natl Acad Sci USA* 103:10046–10051.
21. Nir Y, Hasson U, Levy I, Yeshurun Y, Malach R (2006) *Neuroimage* 30:1313–1324.
22. Damoiseaux JS, Rombouts SA, Barkhof F, Scheltens P, Stam CJ, Smith SM, Beckmann CF (2006) *Proc Natl Acad Sci USA* 103:13848–13853.
23. Honey C, Kotter R, Breakspear M, Sporns O (2007) *Proc Natl Acad Sci USA*, in press.
24. Vincent JL, Patel GH, Fox MD, Snyder AZ, Baker JT, Van Essen DC, Zempel JM, Snyder LH, Corbetta M, Raichle ME (2007) *Nature* 447:83–86.
25. Hebb DO (1949) *The Organization of Behavior* (Wiley, New York).
26. Sporns O, Chialvo DR, Kaiser M, Hilgetag CC (2004) *Trends Cogn Sci* 8:418–425.
27. Sporns O (2002) in *Neuroscience Databases. A Practical Guide*, ed Kotter R (Kluwer, Boston), pp 171–186.
28. Watts DJ, Strogatz SH (1998) *Nature* 393:440–442.
29. Sporns O, Zwi JD (2004) *Neuroinformatics* 2:145–162.
30. Sakai K, Passingham RE (2006) *J Neurosci* 26:1211–1218.
31. Burgess PW (2000) *Psychol Res* 63:279–288.
32. Raichle ME, MacLeod AM, Snyder AZ, Powers WJ, Gusnard DA, Shulman GL (2001) *Proc Natl Acad Sci USA* 98:676–682.
33. Corbetta M, Shulman GL (2002) *Nat Rev Neurosci* 3:201–215.
34. Fincham JM, Carter CS, van Veen V, Stenger VA, Anderson JR (2002) *Proc Natl Acad Sci USA* 99:3346–3351.
35. Fincham JM, Anderson JR (2006) *Proc Natl Acad Sci USA* 103:12941–12946.
36. Woldorff MG, Hazlett CJ, Fichtenholtz HM, Weissman DH, Dale AM, Song AW (2004) *J Cogn Neurosci* 16:149–165.
37. Rushworth MF, Johansen-Berg H, Gobel SM, Devlin JT (2003) *Neuroimage* 20(Suppl 1):S89–S100.
38. Fiez JA (1996) *Neuron* 16:13–15.
39. Koechlin E, Basso G, Pietrini P, Panzer S, Grafman J (1999) *Nature* 399:148–151.
40. Bunge SA, Wallis JD, Parker A, Brass M, Crone EA, Hoshi E, Sakai K (2005) *J Neurosci* 25:10347–10350.
41. Botvinick MM, Cohen JD, Carter CS (2004) *Trends Cogn Sci* 8:539–546.
42. Weissman DH, Gopalakrishnan A, Hazlett CJ, Woldorff MG (2005) *Cereb Cortex* 15:229–237.
43. Rushworth MF, Walton ME, Kennerley SW, Bannerman DM (2004) *Trends Cogn Sci* 8:410–417.
44. Fan J, Kolster R, Ghajar J, Suh M, Knight RT, Sarkar R, McCandliss BD (2007) *J Neurosci* 27:2272–2282.
45. Johnston K, Levin HM, Koval MJ, Everling S (2007) *Neuron* 53:453–462.
46. Kennerley SW, Walton ME, Behrens TE, Buckley MJ, Rushworth MF (2006) *Nat Neurosci* 9:940–947.
47. Crottaz-Herbette S, Menon V (2006) *J Cogn Neurosci* 18:766–780.
48. Etkin A, Egner T, Peraza DM, Kandel ER, Hirsch J (2006) *Neuron* 51:871–882.
49. Bunge SA, Dudukovic NM, Thomason ME, Vaidya CJ, Gabrieli JD (2002) *Neuron* 33:301–311.
50. Fan J, McCandliss BD, Fossella J, Flombaum JI, Posner MI (2005) *Neuroimage* 26:471–479.
51. Gilbert SJ, Spengler S, Simons JS, Steele JD, Lawrie SM, Frith CD, Burgess PW (2006) *J Cogn Neurosci* 18:932–948.
52. Kondo H, Osaka N, Osaka M (2004) *Neuroimage* 23:670–679.
53. Miezin F, Maccotta L, Ollinger J, Petersen S, Buckner R (2000) *NeuroImage* 11:735–759.
54. Fair DA, Schlaggar BL, Cohen AL, Miezin FM, Dosenbach NU, Wenger KK, Fox MD, Snyder AZ, Raichle ME, Petersen SE (2007) *Neuroimage* 35:396–405.
55. Field AP (2001) *Psychol Methods* 6:161–180.